Mathematical Modelling and Analysis
Volume 15 Number 1, 2010, pages 39–54
Doi:10.3846/1392-6292.2010.15.39-54

ISSN 1392-6292 print
ISSN 1648-3510 online
www.vgtu.lt/mma/

# Multigrid Fourier Analysis on Semi-Structured Anisotropic Meshes for Vector Problems*

**F.J. Gaspar, F.J. Lisbona and C. Rodrigo**

*Department of Applied Mathematics. University of Zaragoza*
Pedro Cerbuna, 12, 50009 Zaragoza, Spain
E-mail(*corresp.*): fjgaspar@unizar.es
E-mail: lisbona@unizar.es;carmenr@unizar.es

Received August 31, 2009; revised December 11, 2009; published online February 15, 2010

**Abstract.** An efficient multigrid finite element method for vector problems on triangular anisotropic semi-structured grids is proposed. This algorithm is based on zebra line-type smoothers to overcome the difficulties arising when multigrid is applied on stretched meshes. In order to choose the type of multigrid cycle and the number of pre- and post-smoothing steps, a three-grid Fourier analysis is done. To this end, local Fourier analysis (LFA) on triangular grids for scalar problems is extended to the vector case. To illustrate the good performance of the method, a system of reaction-diffusion is considered as model problem. A very satisfactory global convergence factor is obtained by using a V(0,2)-cycle for domains triangulated with highly anisotropic meshes.

**Keywords:** finite elements, semi-structured triangular grids, geometric multigrid, local Fourier analysis, three-grid analysis, anisotropic meshes.

**AMS Subject Classification:** 65N55; 65F10; 65N30.

## 1 Introduction

One of the most important aspects in the numerical solution of systems of partial differential equations is the efficient solution of the corresponding large systems of equations arising from their discretization. In the 70's, multigrid methods [4, 8] were developed having the nice property that the required work for solving these systems was of the order of the number of unknowns, at least for elliptic problems. Nowadays, these methods are very popular among scientists and they have been extended and applied to more complicated problems, for example see [13]. There are two basic approaches to multigrid solvers: geometric and algebraic multigrid. Whereas in geometric multigrid a hierarchy of grids must be proposed, in algebraic multigrid no information is used

* This research has been partially supported by FEDER/MCYT Projects MTM2007-63204 and the DGA (Grupo consolidado PDIE)

concerning the grid on which the governing PDE is discretized. This approach only uses information contained in the algebraic equations, what makes it more suitable for unstructured grids and for problems with large variations in the coefficients of the PDE. While algebraic multigrid is capable of handling large problems with irregular structure, geometric multigrid always has a lower cost per iteration, because of its ability to take advantage of the geometry within the data structures used. On the other hand, the development of AMG methods for systems of PDEs is far from complete. For example, AMG schemes do not demonstrate their typical efficiency for many current application problems. Some contributions towards the development of AMG methods for systems of PDEs can be found in [7, 11]. For example, in [3], a reaction-diffusion system similar to that considered here is solved by an AMG method, and there it is reported that the convergence factor of the AMG iteration does not scale as is the case in the geometric multigrid methods when the number of pre- and post-smoothing steps increases. An alternative to the use of AMG for unstructured grids is proposed here for relatively complex domains. This methodology is based on considering semi-structured grids, making possible the efficient implementation of a geometric multigrid algorithm.

Geometric multigrid methods strongly depend on their user-chosen components. Particularly, the smoother, transfer operators, number of pre- and post-smoothing steps, type of cycle (e.g. V-cycle versus W-cycle) and so on, have to be selected for each concrete problem. To choose suitable components, a useful tool, introduced by Brandt in 1977 [4], is local Fourier analysis. From the practical point of view, this analysis is very helpful because it provides a very realistic estimate of the asymptotic convergence factor of the multigrid method. The most common approaches of this analysis are the Fourier one-grid (smoothing) and two-grid analysis, however, at least a three-grid analysis must be considered if the influence of the type of cycle or/and the different number of pre- and post-smoothing steps needs to be investigated, see [14, 15].

In many PDE models, the anisotropic behavior of the solution can demand the use of anisotropic grids in order to provide an optimal numerical resolution. Anisotropic meshes are also required if the computational domain has an stretched structure, because in this case the use of more regular grids would imply a big amount of nodes. In practice, the characteristics of this type of grids can seriously influence the convergence of some solvers because they do not take into account the mesh geometry. For some applications the anisotropic grid is slightly modified to a more regular mesh in order to obtain a better performance of the solver. However, geometric multigrid methods by using semi-coarsening or line-wise smoothing are an exception of this behavior and become very efficient solvers on highly anisotropic meshes. As a consequence, the use of semi-structured grids combined with geometric multigrid methods can provide a suitable framework for the efficient resolution of many problems requiring anisotropic meshes. In general, semi-structured grids consist of the construction of a purely unstructured input grid, which is assumed to be the coarsest mesh, and a regular refinement on each patch-wise element. This framework offers additional advantages with regard to the memory requirements. Exploiting the regularity of the grid, geometric multigrid methods

can be implemented using stencil-based operations, that is, if finite element discretizations are considered it is not necessary to construct the global matrix by assembly, drastically reducing the memory required, see [2]. Another interesting point is to use the LFA on triangular grids [5] to choose the good components of the multigrid method for each triangular input block, taking into account the particular geometry of the grid on each patch. This strategy has been performed for scalar problems, and its extension to vector problems is pointed out in this paper. From this analysis, zebra line-type smoothers appear as a good relaxation method for these anisotropic semi-structured grids, providing a very efficient multigrid algorithm.

The structure of the paper is as follows. In Section 2, Fourier two-grid analysis on triangular grids is extended to the case of systems of PDEs and a three-grid analysis is also presented in order to get more insight on the behavior of the multigrid method, in particular to study the different performance of V- and W-cycles and the number of pre- and post-smoothing steps, which can not be shown by the two-grid analysis. Section 3 is devoted to present some LFA results, based on zebra-type relaxation, and some numerical experiments with anisotropic meshes, which appear in a natural way from the characteristics of the problem. In the numerical experiments, it will be seen that a V(0,2) multigrid method seems to be a very good solver for the proposed problems.

## 2 Fourier Analysis

### 2.1 General definitions

Local Fourier Analysis is a powerful tool for the design of efficient multigrid methods on regular structured grids. This analysis is mainly based on the Fourier transform. This technique has been widely used in the framework of discretizations on rectangular grids, and recently a generalization to triangular grids has been proposed in [5] for the scalar case. The key to carrying out this generalization is to write the Fourier transform using coordinates in non-orthogonal bases fitting the structure of the grid. In order to extend the LFA to the case of systems of PDEs, a new expression of the Fourier transform for vector functions is considered.

To this end, we establish a non-orthogonal unitary basis of $\mathbb{R}^2$, $\{\mathbf{e}_1', \mathbf{e}_2'\}$, with $0 < \gamma < \pi$ being the angle between the vectors of the basis. We also consider its reciprocal basis $\{\mathbf{e}_1'', \mathbf{e}_2''\}$, i.e., $(\mathbf{e}_i', \mathbf{e}_j'') = \delta_{ij}$, $1 \le i, j \le 2$, where $(\cdot, \cdot)$ is the usual inner product in $\mathbb{R}^2$ and $\delta_{ij}$ is the Kronecker's delta, see Figure 1. The coordinates of a point in these bases, $\{\mathbf{e}_1', \mathbf{e}_2'\}$ and $\{\mathbf{e}_1'', \mathbf{e}_2''\}$, are $\mathbf{y}' = (y_1', y_2')$ and $\mathbf{y}'' = (y_1'', y_2'')$, respectively, just like $\mathbf{y} = (y_1, y_2)$ in the canonical basis $\{\mathbf{e}_1, \mathbf{e}_2\}$. By applying the changes of variables $\mathbf{x} = \mathbf{F}(\mathbf{x}')$ and $\boldsymbol{\theta} = \mathbf{G}(\boldsymbol{\theta}'')$ to the usual Fourier transform formula, it results in

$$\hat{\mathbf{u}}(\mathbf{G}(\boldsymbol{\theta}'')) = \frac{\sin\gamma}{2\pi} \int_{\mathbb{R}^2} e^{-i\mathbf{G}(\boldsymbol{\theta}'')\cdot\mathbf{F}(\mathbf{x}')} \mathbf{u}(\mathbf{F}(\mathbf{x}'))\, \mathrm{d}\mathbf{x}',$$

and its corresponding back transformation formula with coordinates in a non-

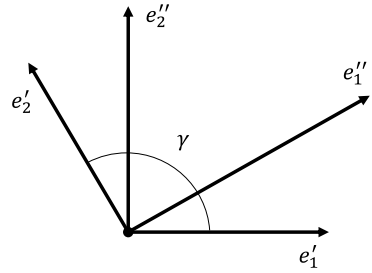


**Figure 1.** Reciprocal bases in $\mathbb{R}^2$.

orthogonal basis, results in the following

$$\mathbf{u}(\mathbf{F}(\mathbf{x}')) = \frac{1}{2\pi \sin\,\gamma} \int_{\mathbb{R}^2} e^{i\mathbf{G}(\boldsymbol{\theta}'')\cdot\mathbf{F}(\mathbf{x}')} \hat{\mathbf{u}}(\mathbf{G}(\boldsymbol{\theta}''))\, \mathrm{d}\boldsymbol{\theta}''.$$

Since the new bases are reciprocal bases, the inner product $\mathbf{G}(\boldsymbol{\theta}'')\cdot\mathbf{F}(\mathbf{x}')$ is given by $\theta_1'' x_1' + \theta_2'' x_2'$. Using previous expressions, a discrete Fourier transform for non-rectangular grids can be introduced. With this purpose, a uniform infinite grid is defined,

$$G_h = \big\{\mathbf{x}' = (x_1', x_2') \,\big|\, x_i' = k_i h_i, \quad k_i \in \mathbb{Z},\ i = 1, 2\big\}, \tag{2.1}$$

where $\mathbf{h} = (h_1, h_2)$ is a grid spacing. We introduce the following inner product between two discrete $(1 \times q)-$grid functions $\mathbf{u}_h$ and $\mathbf{v}_h$, defined on $G_h$,

$$< \mathbf{u}_h, \mathbf{v}_h >= h_1 h_2 \sin\gamma \sum_{\mathbf{x}'\in G_h} \big(\mathbf{u}_h(\mathbf{x}'), \mathbf{v}_h(\mathbf{x}')\big),$$

where $(\cdot,\cdot)$ denotes the usual inner product in $\mathbb{C}^q$. From the definition of this inner product, an associated norm for vector grid functions is obtained, and we can introduce the following space of grid functions

$$(l_h^2(G_h))^q = \{\mathbf{v}_h \,:\, G_h \to \mathbb{C}^q \,|\, \|\mathbf{v}_h\| < \infty\}.$$

Now, for a vector $(1 \times q)-$grid function $\mathbf{u}_h \in (l_h^2(G_h))^q$, the discrete Fourier transform results

$$\hat{\mathbf{u}}_h(\boldsymbol{\theta}'') = \frac{h_1 h_2 \sin\gamma}{2\pi} \sum_{\mathbf{x}'\in G_h} e^{-i(\theta_1'' x_1' + \theta_2'' x_2')} \mathbf{u}_h(\mathbf{x}'),$$

and its inverse Fourier transformation can be defined by

$$\mathbf{u}_h(\mathbf{x}') = \frac{1}{2\pi \sin\gamma} \int_{\boldsymbol{\Theta}_h} e^{i(\theta_1'' x_1' + \theta_2'' x_2')} \hat{\mathbf{u}}_h(\boldsymbol{\theta}'')\, \mathrm{d}\boldsymbol{\theta}'', \tag{2.2}$$

where $\boldsymbol{\theta}'' = (\theta_1'', \theta_2'') \in \boldsymbol{\Theta}_h = (-\pi/h_1, \pi/h_1] \times (-\pi/h_2, \pi/h_2]$ are the coordinates of the point $\theta_1'' \mathbf{e}_1'' + \theta_2'' \mathbf{e}_2''$ in the frequency space.

Considering the scalar Fourier modes, $\varphi_h(\boldsymbol{\theta}'', \mathbf{x}') = \mathrm{e}^{i\theta_1'' x_1'}\,\mathrm{e}^{i\theta_2'' x_2'}$, their vector counterparts are $\boldsymbol{\varphi}_h(\boldsymbol{\theta}'', \mathbf{x}') := \varphi_h(\boldsymbol{\theta}'', \mathbf{x}') \cdot \mathbf{I}$, where $\mathbf{I} = (1, \ldots, 1)^t \in \mathbb{R}^q$, $\mathbf{x}' \in G_h$, and $\boldsymbol{\theta}'' \in \boldsymbol{\Theta}_h$. They give rise to the Fourier space,

$$\mathcal{F}(G_h) = \mathrm{span}\{\boldsymbol{\varphi}_h(\boldsymbol{\theta}'', \cdot) \mid \boldsymbol{\theta}'' \in \boldsymbol{\Theta}_h\}.$$

From (2.2), it follows that each vector discrete function $\mathbf{u}_h(\mathbf{x}') \in (l_h^2(G_h))^q$ can be written as a formal linear combination of the Fourier modes, which are linearly independent discrete functions.

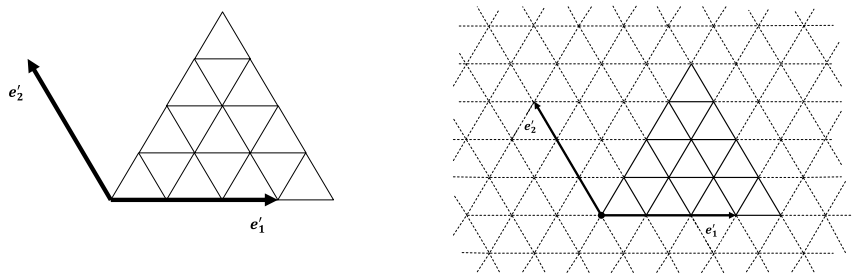


a) b)

**Figure 2.** Grids: a) regular triangular grid on a fixed coarse triangle $\mathcal{T}$, b) its extension to an infinite grid.

Let $\mathcal{T}_h$ be a regular triangular grid on a fixed coarse triangle $\mathcal{T}$ (see the left picture of Figure 2). $\mathcal{T}_h$ is extended to the infinite grid $G_h$ given before, where $\mathbf{e}_1'$ and $\mathbf{e}_2'$ are unit vectors indicating the direction of two of the edges of $\mathcal{T}$, and such that $\mathcal{T}_h = G_h \bigcap \mathcal{T}$ (see the right picture of Figure 2). Neglecting boundary conditions and/or connections with other neighbouring triangles of the coarsest grid, the discrete problem $\mathbf{L}_h \mathbf{u}_h = \mathbf{f}_h$ can be extended to the whole grid $G_h$, and the equations corresponding to a fixed grid point $\mathbf{x}' \in G_h$ are

$$\begin{pmatrix} L_h^{1,1} & \cdots & L_h^{1,q} \\ \vdots & \ddots & \vdots \\ L_h^{q,1} & \cdots & L_h^{q,q} \end{pmatrix} \begin{pmatrix} u_h^1 \\ \vdots \\ u_h^q \end{pmatrix} = \begin{pmatrix} f_h^1 \\ \vdots \\ f_h^q \end{pmatrix},$$

where $L_h^{i,j}$ are assumed to be scalar operators with constant coefficients on the infinite grid $G_h$, in such a way that each of these operators corresponds to a stencil. As is well known, vector Fourier modes $\boldsymbol{\varphi}_h(\boldsymbol{\theta}'', \mathbf{x}')$ are formal eigenfunctions of the discrete operator $\mathbf{L}_h$. More precisely, it is fulfilled

$$\mathbf{L}_h \boldsymbol{\varphi}_h(\boldsymbol{\theta}'', \mathbf{x}') = \widetilde{\mathbf{L}}_h(\boldsymbol{\theta}'') \boldsymbol{\varphi}_h(\boldsymbol{\theta}'', \mathbf{x}') = \begin{pmatrix} \widetilde{L}_h^{1,1}(\boldsymbol{\theta}'') & \cdots & \widetilde{L}_h^{1,q}(\boldsymbol{\theta}'') \\ \vdots & \ddots & \vdots \\ \widetilde{L}_h^{q,1}(\boldsymbol{\theta}'') & \cdots & \widetilde{L}_h^{q,q}(\boldsymbol{\theta}'') \end{pmatrix} \boldsymbol{\varphi}_h(\boldsymbol{\theta}'', \mathbf{x}'),$$

where the $(q \times q)-$matrix $\widetilde{\mathbf{L}}_h(\boldsymbol{\theta}'')$, consisting of scalar Fourier symbols, is the Fourier symbol of $\mathbf{L}_h$. In the following we will denote the Fourier symbol of an operator with $\widetilde{\ }$.

Using standard coarsening, high and low frequency components on $G_h$ are distinguished, in the way that the subset of low frequencies is defined by $\boldsymbol{\Theta}_{2h} = (-\pi/2h_1, \pi/2h_1] \times (-\pi/2h_2, \pi/2h_2]$, and the subset of high frequencies is defined as $\boldsymbol{\Theta}_h \setminus \boldsymbol{\Theta}_{2h}$, (see Fig. 3).

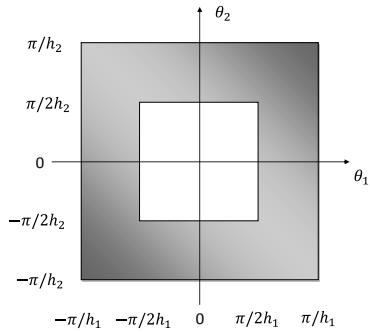


**Figure 3.** High (shaded region) and low (white region) frequencies for standard coarsening.

For simplicity in notation, in the following we will use $\mathbf{x} = (x_1, x_2)$ and $\boldsymbol{\theta} = (\theta_1, \theta_2)$ as the coordinate vectors in the bases $\{\mathbf{e}_1', \mathbf{e}_2'\}$ and $\{\mathbf{e}_1'', \mathbf{e}_2''\}$, respectively.

From these definitions, a smoothing analysis can be performed straightforwardly as in rectangular grids, and smoothing factors for relaxing methods can be well defined. This analysis investigates the influence of a smoothing operator on the high-frequency error components, assuming an ideal coarse-grid operator which annihilates the low-frequency error components and leaves the high-frequency components unchanged. However, if we want to get more insight into the structure of a multigrid algorithm, including the effects of grid transfers in addition to the smoothing by relaxation, it is helpful to perform a two- or three-grid analysis, as we explain next.

### 2.2 Two-grid analysis

In order to investigate the interplay between relaxation and coarse grid correction, which is crucial for an efficient multigrid method, it is convenient to perform a two-grid analysis which takes into account the effect of transfer operators. Let $\mathbf{u}_h^m$ be an approximation of $\mathbf{u}_h$. The error $\mathbf{e}_h^m = \mathbf{u}_h^m - \mathbf{u}_h$ is transformed by a two-grid cycle as $\mathbf{e}_h^{m+1} = \mathbf{M}_h^{2h}\mathbf{e}_h^m$, where $\mathbf{M}_h^{2h} = \mathbf{S}_h^{\nu_2}\mathbf{K}_h^{2h}\mathbf{S}_h^{\nu_1}$ is the two-grid operator, $\mathbf{K}_h^{2h} = \mathbf{I}_h - \mathbf{P}_{2h}^h(\mathbf{L}_{2h})^{-1}\mathbf{R}_h^{2h}\mathbf{L}_h$ is the coarse grid correction operator and $\mathbf{S}_h$ is a smoothing operator on $G_h$ with $\nu_1$ and $\nu_2$ indicating the number of pre– and post–smoothing steps respectively. In the definition of $\mathbf{K}_h^{2h}$, $\mathbf{L}_{2h}$ is the coarse grid operator and $\mathbf{P}_{2h}^h$, $\mathbf{R}_h^{2h}$ are transfer operators from coarse to fine grids and vice versa. The two–grid analysis is the basis for the classical asymptotic multigrid convergence estimates, and the spectral radius $\rho(\mathbf{M}_h^{2h})$ of the operator $\mathbf{M}_h^{2h}$ indicates the asymptotic convergence factor of the

two-grid method.

In order to guarantee that nonsingular Fourier symbols $\widetilde{\mathbf{L}}_h(\boldsymbol{\theta})$ and $\widetilde{\mathbf{L}}_{2h}(2\boldsymbol{\theta})$ are taken, we restrict our considerations to $\tilde{\boldsymbol{\Theta}}_{2h} = \boldsymbol{\Theta}_{2h} \setminus \boldsymbol{\Psi}$, with

$$\boldsymbol{\Psi} = \{\boldsymbol{\theta}^{00} \in \boldsymbol{\Theta}_{2h} \mid \det(\widetilde{\mathbf{L}}_{2h}(2\boldsymbol{\theta}^{00})) = 0, \text{ or } \det(\widetilde{\mathbf{L}}_h(\boldsymbol{\theta}^{ij})) = 0,\ i,j \in \{0,1\}\},$$

where

$$\boldsymbol{\theta}^{10} = \boldsymbol{\theta}^{00} - (sign(\theta_1^{00})\pi/h_1, 0), \quad \boldsymbol{\theta}^{01} = \boldsymbol{\theta}^{00} - (0, sign(\theta_2^{00})\pi/h_2),$$
$$\boldsymbol{\theta}^{11} = \boldsymbol{\theta}^{00} - (sign(\theta_1^{00})\pi/h_1, sign(\theta_2^{00})\pi/h_2),$$

being $\theta_1^{00}$ and $\theta_2^{00}$ the coordinates of $\boldsymbol{\theta}^{00}$ in the basis $\{\mathbf{e}_1'', \mathbf{e}_2''\}$. As is well known, assuming standard coarsening, the coarse grid correction operator $\mathbf{K}_h^{2h}$ couples four Fourier components. Each low frequency $\boldsymbol{\theta}^{00} \in \tilde{\boldsymbol{\Theta}}_{2h}$ is coupled with three high frequencies, $\boldsymbol{\theta}^{10}$, $\boldsymbol{\theta}^{01}$, and $\boldsymbol{\theta}^{11}$, see Figure 4. These frequencies compose the four-dimensional subspaces $\mathcal{F}^4(\boldsymbol{\theta}^{00})$ of $2h$-harmonics, which remain invariant under $\mathbf{K}_h^{2h}$. The same invariance property holds for many well–known smoothers, such as some line-wise smoothers. Therefore, the two–grid operator $\mathbf{M}_h^{2h} = \mathbf{S}_h^{\nu_2}\mathbf{K}_h^{2h}\mathbf{S}_h^{\nu_1}$ also leaves the $2h$–harmonic subspaces invariant, and as a consequence it is equivalent to a block-diagonal matrix, consisting of $(4q \times 4q)$–blocks, denoted by

$$\widehat{\mathbf{M}}_h^{2h}(\boldsymbol{\theta}^{00}) = (\widehat{\mathbf{S}}_h(\boldsymbol{\theta}^{00}))^{\nu_2}\widehat{\mathbf{K}}_h^{2h}(\boldsymbol{\theta}^{00})(\widehat{\mathbf{S}}_h(\boldsymbol{\theta}^{00}))^{\nu_1},$$

with $\boldsymbol{\theta}^{00} \in \tilde{\boldsymbol{\Theta}}_{2h}$, and where the Fourier representation of the relaxation method is a $(4q \times 4q)$-matrix, $\widehat{\mathbf{S}}_h(\boldsymbol{\theta}^{00})$, and the block-matrix representation of the coarse grid correction in the subspace $\mathcal{F}^4(\boldsymbol{\theta}^{00})$ is given by

$$\widehat{\mathbf{K}}_h^{2h}(\boldsymbol{\theta}^{00}) = \widehat{\mathbf{I}}_h - \widehat{\mathbf{P}}_{2h}^h(\boldsymbol{\theta}^{00})(\widehat{\mathbf{L}}_{2h}(\boldsymbol{\theta}^{00}))^{-1}\widehat{\mathbf{R}}_h^{2h}(\boldsymbol{\theta}^{00})\widehat{\mathbf{L}}_h(\boldsymbol{\theta}^{00}) \in \mathbb{C}^{4q\times 4q},$$

being $\widehat{\mathbf{I}}_h$, $\widehat{\mathbf{L}}_{2h}(\boldsymbol{\theta}^{00})$, $\widehat{\mathbf{L}}_h(\boldsymbol{\theta}^{00})$, $\widehat{\mathbf{R}}_h^{2h}(\boldsymbol{\theta}^{00})$ and $\widehat{\mathbf{P}}_{2h}^h(\boldsymbol{\theta}^{00})$ the Fourier representations in $\mathcal{F}^4(\boldsymbol{\theta}^{00})$ of the operators involved in the coarse grid correction. As a consequence, the spectral radius $\rho(\mathbf{M}_h^{2h})$ can be calculated by means of the spectral radius of $(4q \times 4q)$–matrices, so it is possible to determine the asymptotic two–grid convergence factor as:

$$\rho(\mathbf{M}_h^{2h}) = \max_{\boldsymbol{\theta}^{00}\in\tilde{\boldsymbol{\Theta}}_{2h}} \rho(\widehat{\mathbf{M}}_h^{2h}(\boldsymbol{\theta}^{00})).$$

### 2.3 Three-grid analysis

Due to the recursivity of the definition of a k-grid method, the two-grid analysis introduced previously can be generalized to a k-grid analysis. Since a three-grid analysis can be enough to obtain a comprehensive insight into a multigrid method, we are going to introduce this technique which is very useful to see the difference between the different performances of V- and W-cycles and the influence of different number of pre- and post-smoothing steps. Moreover, this analysis gives the opportunity of obtaining a more accurately analysis of the

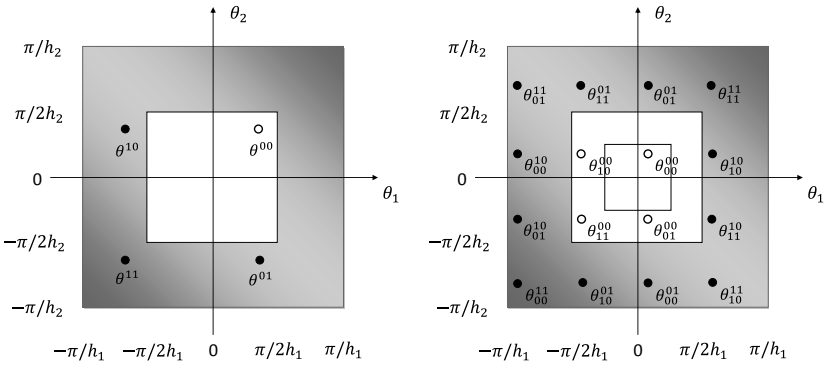


**Figure 4.** Frequencies coupled by a two-grid and a three-grid iteration, which generate the space of 2h- and 4h- harmonics.

coarse-grid correction, and therefore it is especially helpful for problems with difficulties on coarse-grid corrections or when different discretizations are used on coarser grids. The error transformation by a three-grid cycle is given by $\mathbf{e}_h^{m+1} = \mathbf{M}_h^{4h}\mathbf{e}_h^m$, with

$$\mathbf{M}_h^{4h} = \mathbf{S}_h^{\nu_2}\mathbf{K}_h^{4h}\mathbf{S}_h^{\nu_1} = \mathbf{S}_h^{\nu_2}(\mathbf{I}_h - \mathbf{P}_{2h}^h(\mathbf{I}_{2h} - (\mathbf{M}_{2h}^{4h})^\gamma)(\mathbf{L}_{2h})^{-1}\mathbf{R}_h^{2h}\mathbf{L}_h)\mathbf{S}_h^{\nu_1},$$

where $\mathbf{M}_{2h}^{4h}$ is defined as

$$\mathbf{M}_{2h}^{4h} = \mathbf{S}_{2h}^{\nu_2}(\mathbf{I}_{2h} - \mathbf{P}_{4h}^{2h}(\mathbf{L}_{4h})^{-1}\mathbf{R}_{2h}^{4h}\mathbf{L}_{2h})\mathbf{S}_{2h}^{\nu_1},$$

being $\gamma$ the number of two-grid iterations (notice that $\gamma = 1$ corresponds to a V-cycle, whereas $\gamma = 2$ corresponds to a W-cycle).

In order to perform a three-grid analysis we have to take into account that not only in the transition from $G_h$ to $G_{2h}$ but also in the transition from $G_{2h}$ to $G_{4h}$ (where $G_{2h}$ and $G_{4h}$ are the coarse meshes, obtained by standard coarsening, and defined analogously to $G_h$ in (2.1)), four Fourier frequencies are coupled, see Figure 4. Therefore, the three-grid operator couples 16 Fourier frequencies, which set up the subspaces of $4h$-harmonics (composed of four subspaces of $2h$-harmonics), $\mathcal{F}^{16}(\boldsymbol{\theta}^{00})$, $\boldsymbol{\theta}^{00} \in \tilde{\boldsymbol{\Theta}}_{4h} = \boldsymbol{\Theta}_{4h} \setminus \boldsymbol{\Psi}_{4h}$, where $\boldsymbol{\Theta}_{4h} = (-\pi/4h_1, \pi/4h_1] \times (-\pi/4h_2, \pi/4h_2]$, and $\boldsymbol{\Psi}_{4h} = \{\boldsymbol{\theta}^{00} \in \boldsymbol{\Theta}_{4h} \mid \det(\widetilde{\mathbf{L}}_{4h}(4\boldsymbol{\theta}^{00})) = 0, \text{ or } \det(\widetilde{\mathbf{L}}_{2h}(2\boldsymbol{\theta}_{ij}^{00})) = 0, \text{ or } \det(\widetilde{\mathbf{L}}_h(\boldsymbol{\theta}_{nm}^{ij})) = 0,\ i,j,n,m \in \{0,1\}\}$, where

$$\boldsymbol{\theta}_{ij}^{00} = \boldsymbol{\theta}^{00} - (i\pi\, sign(\theta_1^{00})/2h_1, j\pi\, sign(\theta_2^{00})/2h_2)$$
$$\boldsymbol{\theta}_{nm}^{ij} = \boldsymbol{\theta}_{nm}^{00} - (i\pi\, sign((\theta_{nm}^{00})_1)/h_1, j\pi\, sign((\theta_{nm}^{00})_2)/h_2).$$

Hence, this operator can be represented in Fourier space by a block matrix consisting of $(16q \times 16q)-$blocks, and analogously to the definition of the asymptotic convergence factor for the two-grid analysis, we can define it for the three-grid analysis as

$$\rho(\mathbf{M}_h^{4h}) = \max_{\boldsymbol{\theta}^{00} \in \tilde{\boldsymbol{\Theta}}_{4h}} \rho(\widehat{\mathbf{M}}_h^{4h}(\boldsymbol{\theta}^{00})).$$

## 3 Numerical Experiments

In order to see the utility of the previous local Fourier analysis, and in particular of the three-grid analysis, the following reaction–diffusion system with Dirichlet boundary conditions is considered,

$$\begin{cases} -\alpha_1 \Delta p_1 + \kappa(p_1 - p_2) = f_1, \\ -\alpha_2 \Delta p_2 + \kappa(p_2 - p_1) = f_2. \end{cases} \tag{3.1}$$

This system is the stationary version of Barenblatt's equations for fluid flow through fractured porous media, using the double-porosity approach (see [1, 9]). The fluid transport within a porous medium which contains both open fractures and interconnected pore spaces is described by this system of equations giving the pressures, $p_1$ and $p_2$, in each one of the flow systems, that is, $p_1$ in the pores and $p_2$ in the fractures. In both equations there is a term representing an exchange between fissures and pores, which is proportional to the difference of pressures, where the proportionality term $\kappa$ is a transfer coefficient. The diffusion coefficients are given by $\alpha_1 = \dfrac{\kappa_1}{\eta}$ and $\alpha_2 = \dfrac{\kappa_2}{\eta}$, where $\kappa_1$ and $\kappa_2$ are the permeability associated with the pores and fractures respectively, and $\eta$ is the dynamic viscosity of the fluid.

For the numerical experiments presented in this section, the values of the parameters will be taken as $\alpha_1 = 10^{-2}$, $\alpha_2 = 10^{-3}$, and $\kappa = 10^{-4}$, and the triangulation of the computational domains will be done with semi-structured anisotropic grids.

Due to the semi-structured character of the considered mesh, a very efficient storage of the discrete operator is done. Since the grid inside each coarse triangle of the input grid is constructed by regular refinement, only one stencil suffices to represent the discrete operator for inner points to this triangle, avoiding to assemble the corresponding stiffness and mass matrices, which would be composed of rows with the same numerical values but in different locations. Therefore, considering a linear finite element discretization of problem (3.1), the following discrete operator appears for interior points, after normalization:

$$\mathbf{L}_h = \begin{pmatrix} -\alpha_1 \Delta_h + \kappa M_h & -\kappa M_h \\ -\kappa M_h & -\alpha_2 \Delta_h + \kappa M_h \end{pmatrix}, \tag{3.2}$$

where $\Delta_h$, and $M_h$ are the discretizations of the Laplacian and the reactive term, respectively. Besides, also a stencil can be associated with the points lying on the edges of these coarse triangles, and an operator in stencil form similar to (3.2) can be defined for the points associated with each edge. Then, only four stencils are enough to store the discrete operator corresponding to each triangle of the coarsest mesh, whereas it is necessary to assemble the global matrix associated with the vertexes of the coarsest triangulation, due to the totally unstructured character of the coarsest grid. Moreover, the computations necessary to construct these stencils can be simplified by considering a reference stencil computed on a reference hexagon and applying an affine transformation similar to that used in the usual assembly process for FEM. This efficient implementation was recently proposed in [6].

It is well-known that the design of an efficient multigrid method for a given problem strongly depends on the choice of adequate components of the algorithm. Here linear interpolation and its adjoint as the restriction are considered, and the discretization on coarse meshes is done by directly discretizing the equations on each grid. The choice of a suitable smoother is the key for an efficient behavior of the method in many cases. The relaxation process has to be chosen according to the characteristics of both the problem and the structure of the mesh. The shape of the triangles which compose the coarsest mesh has a big influence on the efficiency of the smoother, as it was shown for some scalar problems in [5], where a three-color smoother was preferred for equilateral and quite regular triangles and line-wise smoothers were necessary when the triangles of the coarsest triangulation had some small angle.

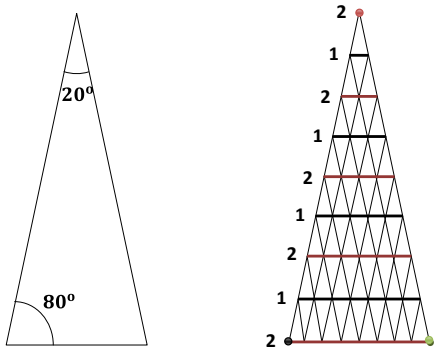


**Figure 5.** Isosceles triangle with common angle $80^{\mathrm{O}}$, and zebra-type smoother corresponding to the smallest angle of the triangle.

As commented before, in the experiments presented in this paper, we deal with triangulations of the domain composed of elongated triangles. So, analogously to the rectangular grids case (see [12]), the anisotropy of the grid requires the use of line-type smoothers associated with the smallest angle of the coarsest triangle. In rectangular grids, zebra-type relaxation (line-wise relaxation analog to point-wise red-black smoothing) is preferred to the lexicographic line-wise relaxation due to the fact that the obtained convergence factors are better than those corresponding to the lexicographic line-wise smoother, see [12]. This zebra-type relaxation consists of the performance of two half-steps: in the first one even lines are relaxed, whereas odd lines are processed in the second half-step, using the updated approximations obtained on the even lines (x-line zebra smoother). It can be done the same with the columns of the grid (y-line zebra smoother). Analogously on triangular grids three zebra-type smoothers can be defined associated with the three directions of the edges of the triangle, and correspondingly with its three vertexes. In Figure 5*b* the zebra-type smoother corresponding to the smallest angle of an isosceles triangle is shown. Approximations at points marked by 1 are updated in the first half-step of the

relaxation, and those marked by 2 in the second one.

These zebra-type smoothers on triangular grids, like standard line-wise smoothers, give better results when they are carried out in the direction of the opposite edge to the smallest angle of the triangle. This behavior can be seen in Figure 6, where for different triangles given in function of two of their angles $\alpha$, and $\beta$, the spectral radius of the three-grid operator, $\rho(M_h^{4h})$, predicted by the 3-grid LFA analysis, with a V-cycle with no pre- and two post-smoothing steps and considering the zebra-smoother associated with the angle $(180^{\text{o}} - \alpha - \beta)$, is depicted. It can be observed that the best values are around 0.05, and they are reached on a wide region corresponding to small values of the angle $(180^{\text{o}} - \alpha - \beta)$.

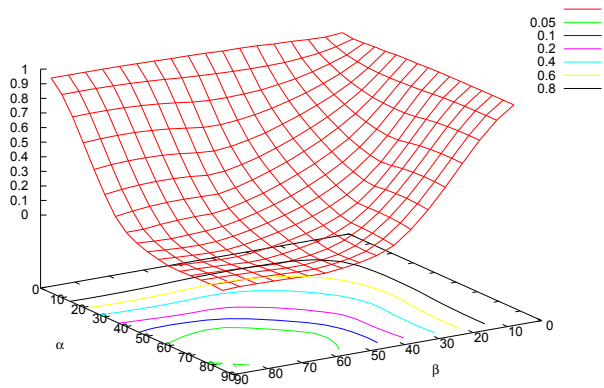


**Figure 6.** Spectral radius $\rho(M_h^{4h})$ for a V(0,2) and zebra-smoother for different triangles in function of two of their angles.

In order to choose an efficient algorithm for model problem (3.1), in Table 1 the behavior of V- and W-cycles with different number of pre- and post-smoothing steps is analyzed. As domain, we consider an isosceles triangle of common angle $80^{\text{o}}$, see Figure 5*a*, which is representative of the type of triangles used on the coarsest triangulations of the computational domains appearing in the numerical experiments, where Dirichlet boundary conditions are considered. The asymptotic convergence factors predicted by a two-grid and a three-grid local Fourier analysis, $\rho_{2g}$, and $\rho_{3g}$, are shown together with the experimentally measured convergence rates $\rho_h(kg)$, that is the asymptotic value of the ratio between the norm of the residuals resulting from two successive k-grid cycles, obtained with a random initial guess and zero right-hand side. In particular, convergence rates for $k = 3$ and $k = 10$ grids, that is $\rho_h(3g)$, and $\rho_h(10g)$, respectively, are presented, by considering the same finest grid resolution. It is observed that the differences in the performance of a V-cycle and a W-cycle are not displayed by the two-grid analysis, whereas the three-grid analysis predicts accurately their different behavior, as well as the differences with regard to the number of pre- and post-smoothing steps. The LFA two-grid and three-grid predictions for the W-cycle are equal, and there is no difference in the behavior of this type of cycle with respect to the number of pre- and post-smoothing

steps. A surprising fact in the performance of the V(0,2)-cycle can be also observed, that is the asymptotic convergence factor given by a three-grid LFA is enough to accurately predict the real asymptotic convergence of the method for any number of grids.

**Table 1.** LFA two–grid, $\rho_{2g}$, and three-grid, $\rho_{3g}$, convergence factors, and experimentally measured asymptotic convergence rates obtained with a zebra-type smoother for an isosceles triangle of common angle $80^{\mathrm{O}}$.

| cycle$(\nu_1, \nu_2)$ | $\rho_{2g}$ | $\rho_{3g}$ | $\rho_h(3g)$ | $\rho_h(10g)$ |
|---|---|---|---|---|
| V(1, 1) | 0.049 | 0.073 | 0.073 | 0.088 |
| V(2, 0) | 0.049 | 0.073 | 0.074 | 0.122 |
| V(0, 2) | 0.049 | 0.048 | 0.047 | 0.047 |
| W(1, 1), W(2, 0), W(0, 2) | 0.049 | 0.049 | 0.048 | 0.048 |

From these results and due to the fact that V-cycles are less expensive than W-cycles, a V-cycle with zero pre- and two post-smoothing steps seems to be a very efficient choice for the resolution of problem (3.1) on a triangular domain with the geometry previously described, when a zebra-smoother associated with the smallest angle of the triangle is used.

Next, some numerical experiments are presented to illustrate the good performance of the proposed algorithm based on a V(0,2)-cycle. First, a homogeneous version of problem (3.1) is solved on the domain depicted in Figure 7.

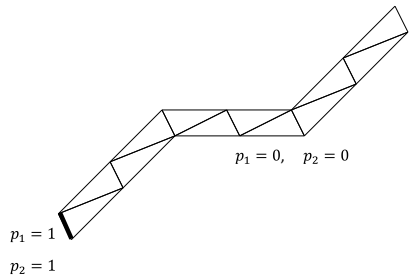


**Figure 7.** Domain problem for the first numerical experiment, with boundary conditions, and coarsest grid consisting of 12 triangles.

Homogeneous Dirichlet boundary conditions are prescribed in the whole boundary except at the left bottom part, where both unknowns are fixed to be equal to one. The domain is composed of three parallelograms with a ratio between their dimensions of about $1:5$. The considered coarsest triangulation, also displayed in this figure, is composed of twelve triangles with small angle of $23.2^{\mathrm{O}}$ or $26.5^{\mathrm{O}}$, what makes suitable the application of zebra-type smoothers. Once this coarsest triangulation is fixed, a regular refinement process is applied to each triangular block until to get the desired fine scale to approximate the solution of the problem. Notice that such an anisotropic meshing leads to significant savings in total number of grid points and the solution costs.

Due to the semi-structured character of the grid, each coarse triangle can

be treated as a different block in the smoothing process. So, it is possible to apply on each triangle the zebra-smoother corresponding to the smallest angle. Moreover, as on each coarse triangle the refinement is done regularly, it is feasible the application of local Fourier analysis in order to obtain the local asymptotic convergence factor corresponding to each triangle, and as a consequence, an estimate of the global convergence factor, taking into account the worst of them. From this analysis for each triangular block, factors of 0.047 and 0.045 for coarse triangles with small angle of $23.2^{\mathrm{O}}$ and $26.5^{\mathrm{O}}$, respectively, are obtained, being therefore the worst 0.047. This means that we expect a factor around this value for the global convergence of the proposed multigrid method.

The obtained multigrid convergence for this problem is shown in Figure 8 for different number of refinement levels, being the stopping criterion that the absolute maximum residual over all unknowns should be less than $10^{-10}$. It can be seen that this convergence is independent of the space discretization parameter, and also that the obtained results are very satisfactory, since the residual is reduced in a few iterations. Moreover, an asymptotic convergence factor about 0.056 is obtained by taking zero right-hand side and a random initial guess, being this value very close to the one predicted by LFA.

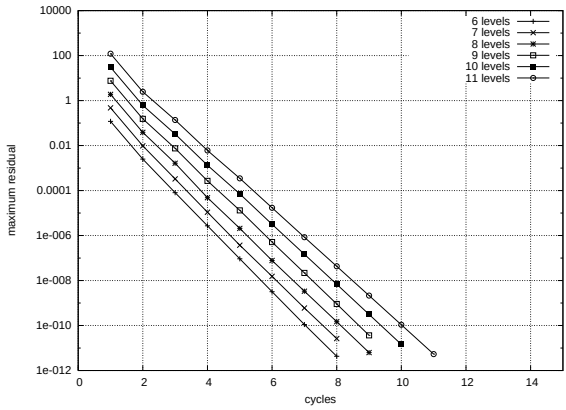


**Figure 8.** Multigrid convergence for model problem (3.1) with V(0,2) using a zebra-type smoother, for the first numerical experiment.

In the second numerical experiment, an example where the solution displays anisotropic behavior, and thus demands the use of anisotropic grids, is studied. Model problem (3.1) is considered with right-hand sides $f_1$ and $f_2$, and Dirichlet conditions such that the exact solution is given by $p_1 = x^2 + 50y^2 + 0.01\cos(\pi(x+y))$, and $p_2 = x^2 + 80y^2 + 0.01\cos(\pi(x+y))$, which exhibit a strong anisotropic performance. If one hopes to provide a good representation of the solution, the triangulation may inevitably produce elements with small angles. The computational domain is taken as the unit square, and the coarsest triangulation must be chosen such that the mesh elements are stretched in the x-direction, as indicated in Figure 9, where the particular coarsest mesh considered in this example is shown. It is composed of 10

triangles with smallest angle around $11^{\mathrm{o}}$, what makes appropriate the use of zebra-type smoothers.

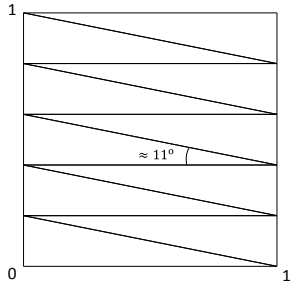


**Figure 9.** Domain problem for the second numerical experiment, and coarsest grid consisting of 10 triangles.

Thus, the same strategy applied to the previous example is suitable for this second experiment, i.e. a V(0,2) with the corresponding zebra-line smoother for each triangle is performed. In Table 2, the number of iterations necessary to reduce the initial residual with a factor of $10^{-10}$, together with the number of elements and the number of unknowns of the problem are shown for different refinement levels. It is observed that the convergence of the method is independent of the number of refinement levels and very satisfactory, due to the fact that the residual is reduced in only 10 iterations.

**Table 2.** Number of multigrid cycles for the resolution of the second numerical experiment with V(0,2) using a zebra-type smoother, for different refinement levels.

| No. of levels | No. of elements | No. of unknowns | No. of cycles |
|---|---|---|---|
| 6 | 10240 | 10626 | 10 |
| 7 | 40960 | 41730 | 10 |
| 8 | 163840 | 165378 | 10 |
| 9 | 655360 | 658434 | 10 |
| 10 | 2621440 | 2627586 | 10 |

For this problem, the asymptotic convergence factor experimentally obtained with a random initial guess and zero right-hand sides is about 0.12. This discrepancy with the predicted LFA factor is due to the difficulties that appear in this type of problems, where line-type smoothers are applied on a grid divided on several blocks, see [10]. In that work, several strategies (extra update of the overlap regions and additional boundary relaxations) were proposed to manage that the convergence rate of multigrid could not be much affected by grid partitioning. In this experiment, we have followed these recommendations together with the use of an over-relaxation parameter in the smoother of value 1.25. Notice that the convergence factors obtained with these strategies are very satisfactory.

## 4 Conclusions

Many problems of interest require extremely anisotropic meshes because either the computational domain is very elongated or the solution of the problem has an anisotropic behavior. It is well-known that the performance of many solvers suffers when this kind of grids are considered. Taking advantage of the fact that geometric multigrid methods on structured grids are an exception, here an effective multigrid method on semi-structured triangular grids, based on a zebra line-type smoother, is proposed. In this algorithm the components of the multigrid method are chosen in function of the shape of each input element of the coarsest grid. With the help of a three-grid Fourier analysis on triangular grids for vector problems, a V(0,2) multigrid cycle is chosen yielding a powerful solver.

## References

[1] G.I. Barenblatt, I.P. Zheltov and I.N. Kochina. Basic concepts in the theory of seepage of homogeneous liquids in fissured rocks. *Prikl. Mat. Mekh.*, **24**:852–864, 1960.

[2] B. Bergen, T. Gradl, F. Hulsemann and U. Ruede. A massively parallel multigrid method for finite elements. *Comput. Sci. Eng.*, **8**:56–62, 2006. Doi:10.1109/MCSE.2006.102.

[3] A. Borzi and G. Borzi. An algebraic multigrid method for a class of elliptic differential systems. *SIAM J. of Scientific Computing*, **25**(1):302–323, 2003. Doi:10.1137/S1064827502411250.

[4] A. Brandt. Multi-level adaptive solutions to boundary-value problems. *Math. Comput.*, **31**:333–390, 1977. Doi:10.2307/2006422.

[5] F.J. Gaspar, J.L. Gracia and F.J. Lisbona. Fourier analysis for multigrid methods on triangular grids. *SIAM J. Sci. Comput.*, **31**(3):2081–2102, 2009. Doi:10.1137/080713483.

[6] F.J. Gaspar, J.L. Gracia, F.J. Lisbona and C. Rodrigo. Efficient geometric multigrid implementation for triangular grids. *J. Comput. Appl. Math.*, 2010. (Article in press)

[7] M. Griebel, M.A. Schweitzer and D. Oeltz. An algebraic multigrid method for linear elasticity. *SIAM J. Sci. Comput.*, **25**(2):385–407, 2003. Doi:10.1137/S1064827502407810.

[8] W. Hackbusch. *Multi-grid methods and applications.* Springer, Berlin, 1985.

[9] P.S. Huyakorn and G.F. Pinder. *Computational methods in subsurface flow.* Academic Press, Inc. Orlando, Florida, 1983.

[10] C.W. Oosterlee. The convergence of parallel multiblock multigrid methods. *Appl. Numer. Math.*, **19**:115–128, 1995. Doi:10.1016/0168-9274(95)00020-U.

[11] J.W. Ruge and K. Stüben. *Algebraic multigrid.* In Multigrid Methods, S.F. McCormick, ed., Frontiers in Appl. Math. 3 (pp. 73–130), SIAM, Philadelphia, 1987.

[12] K. Stüben and U. Trottenberg. *Multigrid methods: Fundamental algorithms, model problem analysis and applications*. In Multigrid Methods, Lecture Notes in Math. 960 (pp. 1–176), W. Hackbusch and U. Trottenberg, eds., Springer-Verlag, Berlin, 1982.

[13] U. Trottenberg, C.W. Oosterlee and A. Schüller. *Multigrid*. Academic Press, New York, 2001.

[14] R. Wienands and W. Joppich. *Practical Fourier analysis for multigrid methods*. Chapman and Hall/CRC Press, 2005.

[15] R. Wienands and C.W. Oosterlee. On three-grid Fourier analysis for multigrid. *SIAM J. Sci. Comput.*, **23**(2):651–671, 2001. Doi:10.1137/S106482750037367X.